Stark fluorescence spectroscopy reveals two emitting sites in the dissipative state of FCP antennas

Md. Wahadoszamen [a,c,*], Artur Ghazaryan [b,1], Hande E. Cingil [a,1], Anjue Mane Ara [a,d], Claudia Büchel [b], Rienk van Grondelle [a], Rudi Berera [a,*]

[a] Division of Physics and Astronomy, Department of Biophysics, VU University Amsterdam, The Netherlands
[b] Institute of Molecular Biosciences, Goethe University Frankfurt, Frankfurt, Germany
[c] Department of Physics, University of Dhaka, Dhaka 1000, Bangladesh
[d] Department of Physics, Jagannath University, Dhaka 1100, Bangladesh

ABSTRACT

Diatoms are characterized by very efficient photoprotective mechanisms where the excess energy is dissipated as heat in the main antenna system constituted by fucoxanthin–chlorophyll (Chl) protein complexes (FCPs). We performed Stark fluorescence spectroscopy on FCPs in their light-harvesting and energy dissipating states. Our results show that two distinct emitting bands are created upon induction of energy dissipation in FCPa and possibly in FCPb. More specifically one band is characterized by broad red shifted emission above 700 nm and bears strong similarity with a red shifted band that we detected in the dissipative state of the major light-harvesting complex II (LHCII) of plants [26]. We discuss the results in the light of different mechanisms proposed to be responsible for photosynthetic photoprotection.

© 2013 Elsevier B.V. All rights reserved.

1. Introduction

Diatoms are unicellular photosynthetic organisms of high ecological importance. Their photosynthetic apparatus resembles that of higher plants, except for the light harvesting proteins, which are called FCPs due to their pigmentation. According to sequence analysis FCPs are membrane intrinsic and three-helix proteins, whereby helices 1 and 3 are similar to the corresponding helices in LHCII of higher plants. FCPs bind Chl a, Chl c and fucoxanthin as their main carotenoid, characterized by an extreme bathochromic shift upon binding to the proteins, absorbing up to 565 nm. In addition diadinoxanthin and diatoxanthin can also be found in smaller amounts. Pigment stoichiometry in FCPs also differs from LHCII. With about 4 fucoxanthins: 4 Chl a:1 Chl c [1], carotenoids are present in much larger amounts as compared to higher plants.

In *Cyclotella meneghiniana* two major FCP complexes named FCPa and FCPb were isolated and characterized [1–7]. FCPa and FCPb display similar features in absorbance, but FCPb binds the more red shifted

fucoxanthins. The two complexes also differ in polypeptide composition and while FCPa is trimeric, FCPb is of higher oligomeric state [2].

Diatoms display a very large magnitude of non-photochemical quenching (NPQ) [8] under high light illumination [9]. NPQ was shown to depend on the de-epoxidation of the xanthophyll diadinoxanthin to diatoxanthin (comparable to the conversion of violaxanthin to zeaxanthin in the xanthophyll cycle in higher plants) [10], triggered by the acidification of the thylakoid lumen. In addition, a class of FCP proteins, known as Lhcx, was shown to be essential for NPQ induction [11], since diatoms do not possess psbS which triggers NPQ in higher plants. While FCPa contains a member of the Lhcx family as one of its subunits, FCPb does not contain Lhcx proteins [3]. Accordingly, the fluorescence yield of FCPa but not of FCPb, was shown to be influenced by the diatoxanthin content and the pH [12,13]. Aggregation of pigment–protein complexes has been used for decades as a model system for in vivo energy dissipation in higher plants [14–16]. Over recent years it has become increasingly clear that protein aggregation may also play a key role in diatoms NPQ. More specifically Miloslavina et al. [17] recorded transient fluorescence kinetics of whole cells at room temperature in the dark and under strong illumination, i.e. under NPQ conditions. They could identify a new component with an additional emission above 700 nm, which was attributed to aggregated FCP complexes, but its specific origin remained unclear so far. Thus, either FPCa or FCPb, or both could be responsible for the long wavelength fluorescence only present under NPQ conditions. While the close distance between FCP

* Corresponding authors at: Division of Physics and Astronomy, Department of Biophysics, VU University Amsterdam, The Netherlands. Tel.: +31 20 59 87426; fax: +31 20 59 87999.
  E-mail addresses: m.d.wahadoszamen@vu.nl (M. Wahadoszamen), r.berera@vu.nl (R. Berera).
  [1] Authors contributed equally.

proteins induced by aggregation may look somewhat artifactual, it is worth noting that the influence of protein distance on the fluorescence yield of FCPs was also demonstrated in proteoliposomes, an environment more akin to the in vivo environment felt by FCPs [13]. In the present study, we applied Stark fluorescence spectroscopy to solubilised (unquenched) and aggregated (quenched) FCPs with the aim to better characterize the emitting specie(s) formed upon induction of fluorescence quenching, more specifically by revealing their excited state electronic structure and dynamics. Stark spectroscopy, which monitors electric field-induced changes in absorption (Stark absorption, SA) or fluorescence (Stark fluorescence, SF), can be used to trace and estimate the change in electrostatic parameters such as permanent dipole moment and molecular polarizability upon optical excitation and/or relaxation [18,19], as well as to probe the rates of excited state reactions and deactivations and their response to an electric field [20,21]. The determination of these parameters is pivotal for the characterization of the excited state electronic structure and dynamics of the molecule or molecular aggregate under study. Stark spectroscopy is particularly useful for the identification of charge transfer (CT) states [8] since CT states are typically associated with a large electric dipole moment and thus exhibit highly selective and sensitive response to the externally applied electric field [21–24]. Inter alia, Stark spectroscopy is also a very useful tool to unravel the spectral constituents of isolated molecules or aggregates which, because of having closely lying energy levels, yield a single spectral profile in conventional spectroscopy [19,23,25,26].

2. Experimental

2.1. Culturing of diatoms and preparation of FCP complexes

The diatom *C. meneghiniana* (Culture Collection Göttingen, strain 1020-1a) was grown under a low light (40 μmol photons m^{-2} s^{-1}) regime with 16 h light and 8 h dark in culture medium according to Provasoli et al. [27] supplemented with 2 mM silica. Cells were inoculated with an initial concentration of 5×10^5 cells/mL and harvested after 7 days of culturing in the early light phase by centrifugation. Thylakoid membranes were isolated by several centrifugation steps after breaking the cells in a bead mill according to reference [2], except that they were finally resuspended in a washing buffer containing EDTA to reduce chlorophyllase activity (10 mM Mes, 2 mM KCl, 5 mM EDTA, pH 6.5, according to Beer et al. [3]). Thylakoids containing 0.5 mg total Chl a (0.25 mg/mL) were solubilized for 20 min on ice with 20 mM β-dodecyl maltoside (β-DDM, Glykon, Germany) (1 mol Chl a:70 mol β-DDM). A pool of FCP complexes (FCPp) was then isolated using sucrose density centrifugation [2], whereby the lower FCP band, which is a mixture of FCPa and FCPb, was taken for the SF experiments. FCPa and FCPb were separated directly from solubilised thylakoids by ion exchange chromatography in buffer 1 (25 mM Tris, 2 mM KCl, 0.03% β-DDM (w/v), pH 7.4) according to Beer et al. [3] followed by ultracentrifugation (27,000 rpm, 4 °C) to remove remaining contaminations from photosystems [12]. After preparation, all FCP complexes were washed once using buffer 1 without β-DDM and then concentrated using filtration devices with a 30 kD cutoff (Centripreps). For the preparation of quenched, i.e. aggregated, FCPs, several steps of dilutions and concentrations were done followed by dialysis against buffer 1 without β-DDM (38 h, 4 °C). Afterwards, the quenched state of FCP (FCPp, FCPa and FCPb) samples was adjusted by incubation with 50 mg of bio-beads (SM-2 adsorbent, Bio-Rad), allowing the reduction of the fluorescence yield by the desired amount (5-fold for FCPp and FCPa and 4-fold for FCPb).

2.2. Stark spectroscopy

The Stark samples of unquenched FCP were prepared by suspending it in a buffer containing 0.01 M Mes with pH-6.5, 0.002 M KCl and 0.03% β-DDM. The resulting samples were then diluted with 57–60% (v/v)

glycerol to produce transparent glasses at 77 K. The Stark sample preparation for quenched FCP was the same as for unquenched FCP; however, in this case part of the detergent, i.e. 0.03% β-DDM was removed until the desired amount of fluorescence quenching was reached. SF spectroscopy was performed on frozen FCPp, FCPa and FCPb glasses at 77 K in a cell consisting of two glass slides coated with Indium Tin Oxide (ITO) electrodes on their inner surfaces and glued together with double sided sticky tape (Sellotape). The optical path length of the resulting cell is therefore determined by the thickness of the sticky tape which in the present study was about 110 μm. The SF measurements were carried out on a homebuilt setup, similar to the one described in [19,28,29]. Briefly, the excitation wavelength is selected by dispersing the white light continuum of a Xenon lamp (Oriel) through a monochromator. The excitation beam hits the sample at an angle of 45°. The sample is immersed into the liquid N$_2$ chamber of an Oxford cryostat (DN1704) having strain free quartz optical windows. A sinusoidal AC voltage with a modulation frequency of 80 Hz is applied to the sample and both the fluorescence (F) and SF signals are recorded simultaneously by a lock-in amplifier (SR850) at the second harmonic of the modulation frequency. The recorded SF signal is multiplied by $2\sqrt{2}$ to convert it to an equivalent dc voltage and finally the SF spectrum is obtained by plotting the SF signal as a function of wavelength. The polarization between the electric field and the excitation wavelength was set at magic angle (54.7°). For the three samples, FCPp, FCPa and FCPb, the F and SF signals were recorded simultaneously at 77 K with an excitation wavelength of 461 nm. At this wavelength the amplitude of the corresponding SA signal is almost zero for all samples (the SA spectrum of unquenched and quenched FCPp, FCPa and FCPb is displayed in Fig. S1 of the Supporting information). This choice of excitation wavelength is made to avoid interference from SA signals during the SF measurement. For the sake of easier comparison the SF spectra reported in Fig. 1 to 6 are scaled to a field strength of 1 MV cm^{-1}, even though the actual field strength used during the measurements had magnitude in the range 0.30 to 0.50 MV cm^{-1}.

2.3. Data analysis

The analysis of the SF data is conventionally done by using the so-called Liptay formalism. According to this formalism, the SF intensity of randomly oriented and spatially immobilized chromophores in rigid matrices can be expressed, under the simplified assumption that the interaction among the emissive chromophores can be neglected, as the weighted sum of the zeroth, first, and second derivatives of the corresponding F spectrum [19,20,29–31]:

$$\frac{2\sqrt{2}\Delta F(\nu)}{F_{max}} = (f\mathbf{F_{ext}})^2 \left\{ A_\chi F(\nu) + B_\chi \nu^3 \frac{d\left[F(\nu)/\nu^3\right]}{d\nu} + C_\chi \nu^3 \frac{d^2\left[F(\nu)/\nu^3\right]}{d\nu^2} \right\}$$

(1)

where F_{max} is the maximum F intensity, $\mathbf{F_{ext}}$ is the intensity of the externally applied electric field, ν is the energy in wavenumber, χ is the experimental angle between the direction of $\mathbf{F_{ext}}$ and the electric vector of the excitation light, and f is the internal field correction factor used to estimate the magnitude of the electric field at the chromophore(s) site, $\mathbf{F_{int}}$; thus $\mathbf{F_{int}} = f\mathbf{F_{ext}}$. The zeroth derivative component reflects the field-induced change in emission intensity arising mostly from field-induced tuning of the rates of nonradiative deactivations competing with the F process; hence the weight of the Zeroth Derivative Contribution (denoted hereafter as ZDC) reveals important information about the dynamics of the molecule or molecular aggregate under investigation [20,24]. Besides, the first and second derivative components, which reflect the field-induced spectral shift and spectral broadening, respectively, often reveal precise information about the electronic structure, more specifically changes in molecular polarizability (Δα) and molecular dipole moment (Δμ) between the ground and

excited states connected by the optical transition, respectively [19,20,24]. At the magic angle ($\chi = 54.7°$) the coefficients, B_χ and C_χ can be expressed as [19]:

$$B_{54.7°} = \frac{\Delta\alpha}{2hc} \tag{2}$$

$$C_{54.7°} = \frac{(\Delta\mu)^2}{6h^2c^2}. \tag{3}$$

Therefore upon fitting the SF spectrum with a linear superposition of the derivatives of the corresponding F spectrum and computing the coefficients of the first and second derivatives, one can extract the values of $\Delta\alpha$ and $\Delta\mu$ from the above two equations. Note that to fit the SF spectrum of QFCP, the necessary deconvolution of the F spectrum to the constituent bands is done by a simple deconvolution technique using Igor software routine where, except the band $b2$, the deconvoluted bands are synthesized using either a single or a linear combination of symmetric Gaussians with suitable widths which yields a good simultaneous fit of the F and the SF spectra. To produce the $b2$ band, the emission lineshape of FCP is used.

3. Results

3.1. SF spectroscopy on FCPp

Fig. 1a and b display the normalized F and SF spectra of a pool of unquenched and quenched FCP complexes, a mixture of FCPa and FCPb, denoted hereafter as FCPp and QFCPp, respectively. FCPp exhibits a sharp and well defined band with a peak at 675 nm due to excitonic emission accompanied by a broad tail (vibrational progression) with a
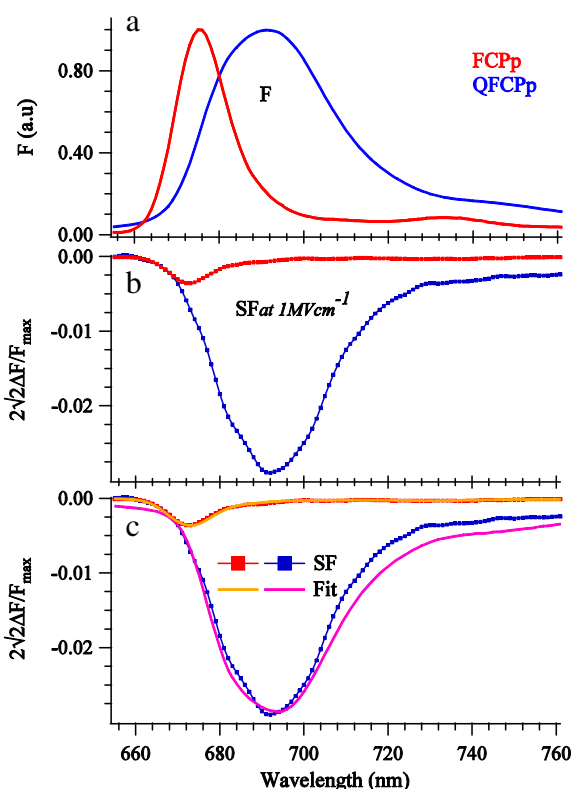

Fig. 1. (a) F and (b) SF spectra of FCPp (red curves) and QFCPp (blue curves) measured in a glycerol/buffer glass at 77 K with excitation wavelength 461 nm. All SF spectra are normalized to the field strength of 1 MV cm^{-1} and to the F intensity at the observed peak maximum. (c) The corresponding fits of the SF spectra obtained by the weighted superposition of the derivatives of the observed F spectrum (without deconvolution) are shown by the solid yellow and magenta lines for FCPp and QFCPp, respectively.

peak at around 735 nm. The F spectrum of QFCPp on the other hand is relatively broad with a peak at 691 nm and a broad tail extending up to the end of the spectral window. Note that QFCPp was about 5 times quenched relative to FCPp. In both cases, the SF spectrum, commonly defined as the difference between the F spectra measured with and without electric field, is characterized by negative intensity with a shape very similar to the corresponding F spectrum. The close similarity between the F and SF spectra indicates that the main effect of the applied electric field is the modulation of the F yield. The negative sign of the SF signal implies a field-induced reduction of F yield in both samples. In addition, the SF peaks of FCPp and QFCPp are blue and red shifted by 2 and 1 nm respectively, compared to their F peaks, showing that the field-induced peak shift in the SF spectra is small. However, as far as the magnitude is concerned, QFCPp gives 8 times larger SF compared to FCPp. This demonstrates an exceptionally high sensitivity of the F state to the applied electric field in QFCPp, even higher than that observed for a comparable band in quenched LHCII [26].

To reveal the underlying excited state's electronic structure and dynamics, the SF spectra of FCPp and QFCPp were analyzed using the simplest Liptay formalism described above. Fig. 1c shows the results. In both cases, the linear superposition of the derivatives of the F spectrum (without deconvolution) was used in the fitting protocol. One can see from the figure that this protocol could reproduce well the SF spectrum of FCPp throughout the entire wavelength region. The analysis thus yielded a single set of molecular (electronic and ZDC) parameters, the magnitudes of which are compiled in Table 1. This result suggests that, likewise various non-interacting photoactive chromophores [24], the F of FCPp originates from a single excited electronic state throughout the measured spectral window. Most likely this state corresponds to the lowest exciton state of the complex. To the contrary, if we look at the fit of the SF spectrum of QFCPp, a clear mismatch is readily apparent throughout most of the spectral region, especially around 660–670 nm, 680–688 nm and 703–760 nm. This observation suggests that the SF analysis of QFCPp is not so simple as that of FCPp. The clear mismatch in fact indicates that the F lineshape of QFCPp does not originate from a single emission band. In this regard, the mismatch around 660–670 nm most likely results from scattering of the excitation beam, the extent of which is very small as one can see by looking at Fig. 1a. The observed intensity in the lower wavelength tail of QFCPp F can thus be considered to be a superposition of F emission and scattering, whose intensity is essentially unaffected by the applied electric field. On the other hand, since the sample is nonselectively excited at 461 nm, energy migration from bluer absorbing chlorophyll pools takes place on different timescales. Since the measurements are done at cryogenic temperature these energy transfer processes are most likely competing with F emission. We thus suggest that the F spectrum of QFCPp in the lower wavelength region around 680 nm contains some contribution from bluer emitting chlorophyll pools. It is also possible that a small fraction of unquenched FCPs is present in the sample preparation which would also contribute to emission in the same spectral region. In addition, one can easily see that the longer wavelength tail of the 691 nm band of QFCPp (720–765 nm region) constitutes a shallow, broad, and distinct band shape. This tail somewhat resembles the vibrational progression of the observed 691 nm band. If this were the case, likewise FCPp, which has a broad vibrational progression peaking around 735 nm as mentioned above, one would expect a satisfactory fit of the SF spectrum throughout the whole wavelength region simply by a linear superposition of the derivatives of the observed F spectrum. The clear mismatch in the longer wavelength region of the SF spectrum in Fig. 1c thus indicates that the shallow band is not the vibrational progression of the 691 nm band but must arise from a different excited electronic state characterized by a distinct set of electronic and ZDC parameters compared to those associated with the 691 nm band. With the information discussed above at hand, the F spectrum of QFCPp was deconvoluted into four major bands designated as $b1p$, $b2p$, $b3p$, and $b4p$ as shown in Fig. 2a. The $b1p$ band, which is a

broad single symmetric Gaussian peaking at 661 nm, reflects the contribution from scattering, and the *b2p* band originates from emission of bluer absorbing chlorophylls where, during energy transfer to the quenching site, some of the energy is lost via F emission. In our fitting scheme we assume the *b2p* band, which peaks at 680 nm, to be the weighted amplitude of the spectral profile obtained by shifting the emission spectrum of FCPp as a whole by 5 nm to the red. While this is probably a reasonable approximation, the real spectral shape of the *b2p* band is likely to be narrower since it possibly originates from a subpopulation of bluer-emitting pigments. Note that the shift of FCPp emission to the red is necessary to fit the shallow band structure of the QFCPp emission around 680 nm. This supports the interpretation that the signal in this wavelength region originates from bluer emitting pigments at the level of which energy transfer and fluorescence compete. The *b3p* band, which has a peak at 692 nm and is a linear combination of five symmetric Gaussians peaking at 690, 697, 702, 717, and 760 nm, and *b4p*, which is a broad single symmetric Gaussian peaking at 736 nm, are considered to be the emission bands of species appearing upon aggregation of FCPp. Note that, as for QFCPp, the F spectrum in the region between the *b2p* and *b4p* bands has a rather inhomogeneously broadened lineshape and five symmetric Gaussians are necessary to produce the *b3p* band. Using a single skewed Gaussian to produce the *b3p* leads to comparable molecular parameters (cf. Table 1 of the ESI and Table 1 of the main text) but to a worse fit of the SF spectrum (cf. Fig. S2 of the ESI). The SF spectrum could then be satisfactorily reproduced by the linear superposition of the derivatives of the *b2p*, *b3p* and *b4p* bands. Since the *b1p* band is attributed to scattering and remains essentially unaffected by the applied electric field, its derivatives were not used in the fitting protocol. The obtained fit is shown by the solid pink line in Fig. 2b together with the SF spectrum (blue square dotted line). Note that in this figure and hereafter in Figs. 4 and 6, the residuals (Raw spectrum–Fit) are shown on top of each panel. The molecular parameters evaluated from the derivative contributions of the deconvoluted bands are compiled in Table 1 together with those obtained from the analysis of unquenched FCPp.

We see from the table that, for FCPp, the analysis yields nonzero ZDC (-0.0033 at a field strength of 1 MV cm^{-1}) and $\Delta\alpha$ (7.16 [Å^3 / f^2]), and zero $\Delta\mu$. The obtained zero magnitude of $\Delta\mu$ indicates that the F of FCPp is not accompanied by a measurable CT character and the rather small magnitude of ZDC together with its negative sign indicates that the applied electric field makes the rates of the associated nonradiative deactivation slightly larger compared to those corresponding to radiative deactivation. Similarly, for *b2p* of QFCPp, the analysis yields the same value of $\Delta\alpha$ (-7.16 [Å^3 / f^2]) and $\Delta\mu$ (0.00 [D / f]), but a 4.5 times larger value of ZDC (-0.015 at 1 MV cm^{-1}) compared to FCPp. For *b3p*, the analysis yields 9.5 times larger ZDC (-0.032 at 1 MV cm^{-1}), almost the same magnitude of $\Delta\alpha$ (-10.74 [Å^3 / f^2]) as for FCPp and nonzero $\Delta\mu$ (1.03 [D / f]). Since $\overline{b3p}$ is considered to be the emission of the first quenching site of FCPp, the nonzero value of $\Delta\mu$ indicates that the associated state possesses a measurable CT character. The obtained large negative amplitude of ZDC indicates that the rates of nonradiative deactivation associated with this state (*b3p* band) are highly accelerated by the external electric field. On the other hand, the analysis of *b4p* yields very large values of both $\Delta\alpha$ (-214.75 [Å^3 / f^2]) and $\Delta\mu$ (8.00 [D / f]) and very small amplitude of the ZDC (-0.0005 at 1 MV cm^{-1}). The estimated values of $\Delta\alpha$ and $\Delta\mu$ for *b4* are about 30 ($=214.13$ / 7.16) and 8 ($=8$ / 1.03) times larger respectively, in terms of absolute magnitude compared to the ones obtained for *b3p*. The remarkably large magnitude of the estimated electronic parameters ($\Delta\alpha$ and $\Delta\mu$) indicates that the state associated to the *b4p* band has exceptionally strong CT character. The very small amplitude of ZDC of *b4p* indicates that the rate of associated nonradiative deactivation is only slightly modulated by the electric field. In conjunction with the analysis of the SF spectrum of unquenched FCPp that gave zero $\Delta\mu$, we can say that the obtained nonzero value of $\Delta\mu$ for both *b3p* and *b4p* bands of QFCPp is a direct consequence of the aggregation and ensuing fluorescence quenching of the FCPp antenna

complex. We conclude that aggregation of FCPp results in two new emissive species which, because of having very different electronic and ZDC parameters, are clearly resolved in the SF spectrum. To gain more insight into the origin of the new emissive bands we carried out SF spectroscopy on unquenched and quenched, pure FCPa and FCPb preparations.

3.2. SF spectroscopy on FCPa

Fig. 3a and b display the F and SF spectra of both trimeric FCPa, denoted hereafter as FCPa and quenched (about 5 times) aggregated FCPa (QFCPa). The F spectrum of FCPa exhibits a sharp band peaking at 676 nm (excitonic emission) accompanied by a broad tail (vibrational progression) having a peak around 735 nm. The F spectrum of QFCPa on the other hand is broader with a peak at 691 nm and a structured tail extending up to the end of the measured spectral window. Once again, the shape of the SF spectrum of both FCPa and QFCPa is similar to the corresponding F spectrum. In addition, the SF peaks of FCPa and QFCPa are blue and red shifted respectively by 1 and 2 nm compared to their F peaks and QFCPa produces almost 7 times larger SF compared to FCPa.

Fig. 3c displays the results of the analysis where the SF spectrum of FCPa and QFCPa was modeled by a linear combination of the derivatives of the observed F spectrum without deconvolution. Like for FCPp, the linear combination of the derivatives of the observed F spectrum could reproduce well the SF spectrum of FCPa. This is not the case for QFCPa where the fitting leads to a clear mismatch between the fit and the SF spectrum in the higher wavelength region. Following the fitting procedure we applied to QFCPp, we deconvoluted the F spectrum of QFCPa into four major bands designated as *b1a*, *b2a*, *b3a*, and *b4a* (Fig. 4a). The bands *b1a*, which is a broad single symmetric Gaussian peaking at 660 nm and *b2a*, with peak around 681 nm, are considered to be the contribution of scattering and emission from bluer absorbing Chls. Like for
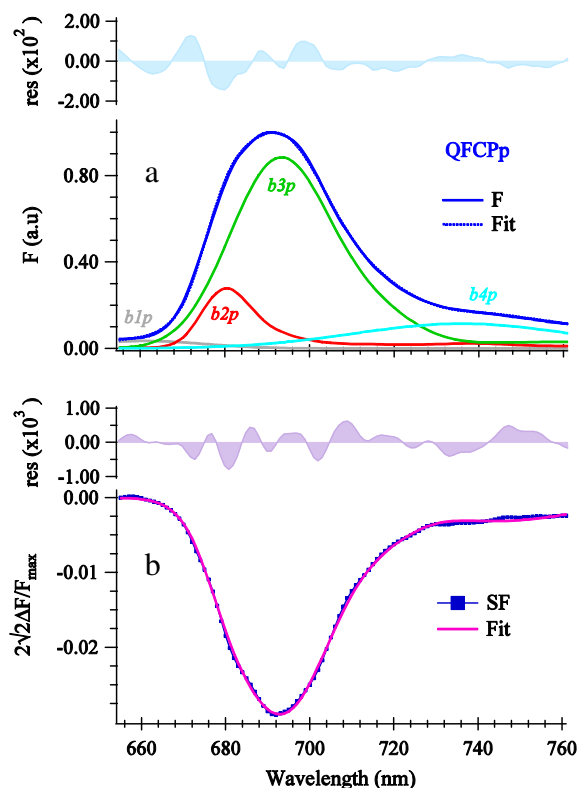

Fig. 2. (a) The F spectrum of QFCPp and the corresponding fit (blue dotted line). The fit of F spectrum was obtained by the linear combination of four bands *b1p*, *b2p*, *b3p* and *b4p*. (b) SF spectra and the corresponding fit (solid magenta line). The fit of the SF spectrum was obtained by the weighted superposition of the derivatives of all the deconvoluted bands except *b1p*. The residual (Raw spectrum–Fit) is shown on top of each panel.

QFCPp, the spectral bandshape of the FCPa emission shifted as a whole by 5 nm to the red was used to produce *b2a*. The bands *b3a*, which has peak at 692 nm and is produced by a linear combination of five symmetric Gaussians peaking at 689, 702, 704, 721, and 770 nm, and *b4a*, which is a broad single symmetric Gaussian peaking at 740 nm, are considered to be the emission bands of emissive species that result from aggregation of FCPa. Fig. 4b shows the resulting fit of the SF spectrum while the molecular parameters are compiled in Table 2 together with those obtained from the analysis of unquenched FCPa. As one can see in the figure, the modeling led to a very good fit of the SF spectrum of QFCPa.

We can see from the table that for FCPa, likewise for FCPp, the analysis gives nonzero ZDC (−0.011 at 1 MV cm^{-1}) and $\Delta\alpha$ (12.53 [$Å^3 / f^2$]), and zero $\Delta\mu$. The analysis of QFCPa yields 7 times larger magnitude of ZDC (−0.071 at 1 MV cm^{-1}) for *b2a* and almost identical values for $\Delta\alpha$ (−10.74 [$Å^3/f^2$]) and $\Delta\mu$ (0.00 [D / f]) compared to FCPa. Furthermore, for *b3a*, the analysis yields 7 times larger magnitude of ZDC (−0.071 at 1 MV cm^{-1}), 2 times larger magnitude of $\Delta\alpha$ (−25.05 [$Å^3 / f^2$]) compared to *b2a* and nonzero $\Delta\mu$ (2.53 [D / f]). The fairly large magnitude of $\Delta\mu$ suggests that *b3a* bears significantly large CT character, larger than the analogous *b3p* band of QFCPp. On the other hand, the analysis of *b4a* yields very large values of both $\Delta\alpha$ (−286.33 [$Å^3 / f^2$]) and $\Delta\mu$ (11.30 [D / f]) and relatively small amplitude of the ZDC (−0.022 at 1 MV cm^{-1}). The estimated values of $\Delta\alpha$ and $\Delta\mu$ for *b4a* are about 27 (286.33/10.74) and 5 (11.30/2.53) times larger in terms of absolute magnitude compared to the ones obtained for *b3a*.

3.3. SF spectroscopy on FCPb

Fig. 5a and b display F and SF spectra of both oligomeric FCPb, denoted hereafter as FCPb and quenched (about 4 times) FCPb (QFCPb). The F
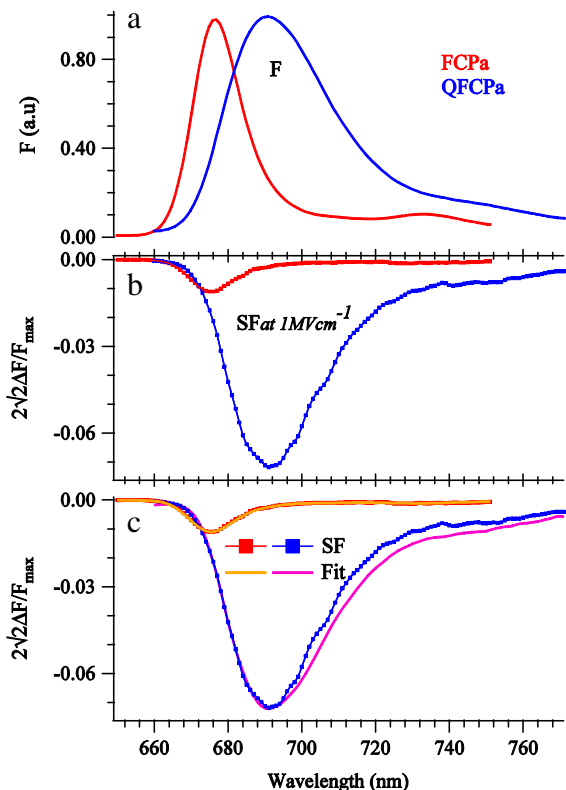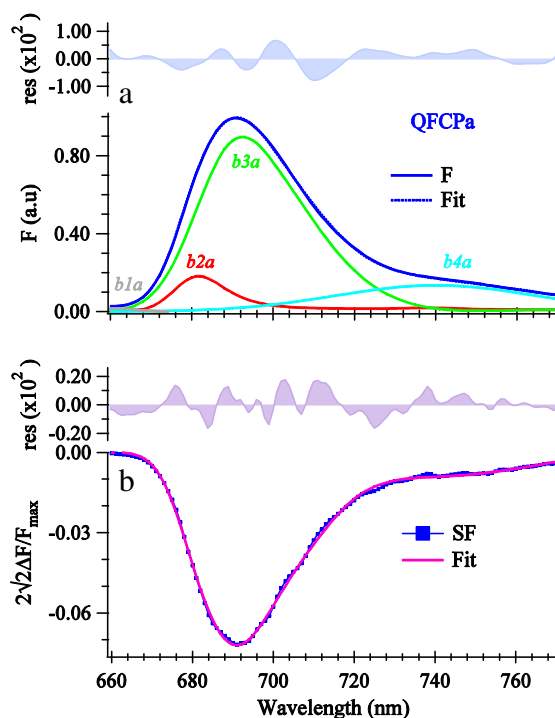

Fig. 4. (a) The F spectrum of QFCPa and the corresponding fit (blue dotted line). The fit of F spectrum was obtained by the linear combination of four bands *b1a*, *b2a*, *b3a*, and *b4a*. (b) SF spectra and the corresponding fit (solid magenta line). The fit of SF spectrum was obtained by the weighted superposition of the derivatives of all the deconvoluted bands except *b1a*. The residual (Raw spectrum–Fit) is shown on top of each panel.

spectra of FCPb and QFCPb resemble those described above for FCPp and FCPa and the SF spectra are similar to the corresponding F spectra. The SF peaks of FCPb and QFCPb are blue and red shifted by 1 and 5 nm respectively, when compared to their F peaks. In this case, QFCPb produces 2.3 times larger SF compared to FCPb.

Fig. 5c displays the results of an analysis where the SF spectrum of FCPb and QFCPb was modeled by the linear combination of the derivatives of the observed F spectrum without deconvolution and again only the spectrum of the unquenched sample could be well reproduced with this approach. However, unlike FCPp and FCPa, the mismatch between the fit and the data is smaller for QFCPb. In order to obtain a better fit of the QFCPb data, the F spectrum was deconvoluted into the constituent bands as shown in Fig. 6a; three major bands designated as *b1b*, *b2b*, and *b3b* were employed in the fit. The bands *b1b* and *b2b* resemble their counterparts in QFCPa and QFCPp. On the other hand, the *b3b* band, which peaks at 694 nm and is composed of a linear combination of six symmetric Gaussians peaking at 673, 685, 695, 710, 718, and 738 nm is considered to be the emission band of the species created upon aggregation of FCPb. The analysis scheme depicted in Fig. 6b resulted in a reasonably good fit of the SF spectrum of QFCPb over the whole spectral region though a small mismatch is still present in the long wavelength region above ~710 nm. The obtained fit is shown by the solid magenta line in Fig. 6b. The molecular parameters evaluated from the derivative contributions of the deconvoluted bands are reported in Table 3 together with those obtained from the analysis of unquenched FCPb. Note that, like for QFCPp and QFCPa, we can also consider a separate (relatively broad) *b4p/b4a*-like band (denoted as *b'4b*) to treat the flat emission of QFCPb around 740 nm (cf. Fig. S3 of the ESI). Although this approach slightly improves the quality of the fit of the SF spectrum above ~710 nm (cf. Fig. S3 of the ESI), it yields essentially the same magnitudes of the molecular parameters (cf. Table 2 of the ESI) for the *b'3b* and *b'4b* bands. Most likely because of the overall small contribution of the *b'4b* band to the fit, our analysis does not allow us to clearly separate it from the *b'3b* band.

Fig. 3. (a) F and (b) SF spectra of FCPa (red curves) and QFCPa (blue curves) measured in a glycerol/buffer glass at 77 K with excitation wavelength 461 nm where the amplitude of the SA signal was almost zero. All the SF spectra are normalized to the field strength of 1 MV cm^{-1} and to the F intensity at the observed peak maximum. (c) The corresponding fits of the SF spectra obtained by the weighted superposition of the derivatives of the observed F spectrum (without deconvolution) are shown by the solid yellow and magenta lines for FCPb and QFCPb, respectively.
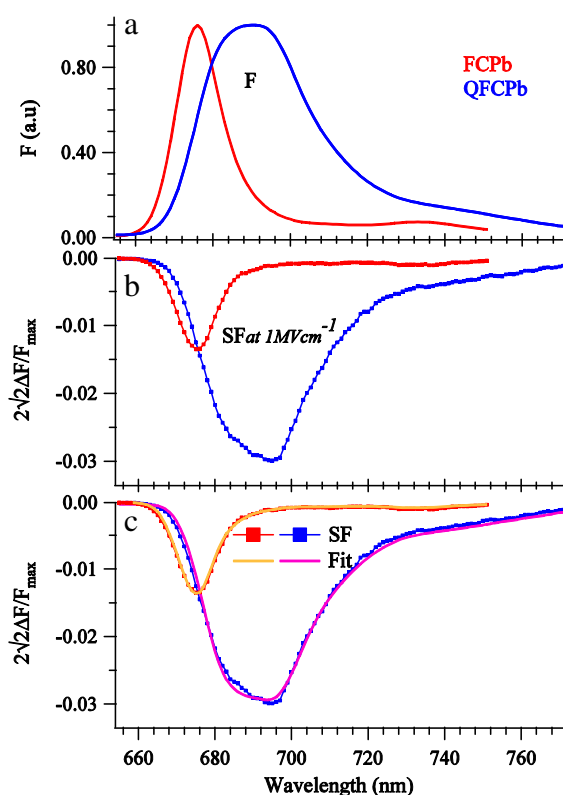
Fig. 5. (a) F and (b) SF spectra of FCPb (red curves) and QFCPb (blue curves) measured simultaneously in a glycerol/buffer glass at 77 K with excitation wavelength 461 nm where the amplitude of the SA signal was almost zero. All the SF spectra are normalized to the field strength of 1 MV cm^{-1} and to the F intensity at the observed peak maximum. (c) The corresponding fits of the SF spectra obtained by the weighted superposition of the derivatives of the observed F spectrum (without deconvolution) are shown by the solid yellow and magenta lines for FCPb and QFCPb, respectively.

Fig. 6. (a) The F spectrum of QFCPb and the corresponding fit (blue dotted line). The fit was obtained by the linear combination of three bands b1b, b2b, and b3b. (b) SF spectra and the corresponding fit (solid magenta line). The fit was obtained by the weighted superposition of the derivatives of all the deconvoluted bands except b1b. The residual (Raw spectrum–Fit) is shown on top of each panel.

We can see from the table that the analysis of FCPb yields nonzero value for ZDC (−0.0115 at 1 MV cm^{-1}) and $\Delta\alpha$ (10.74 [Å^3 / f^2]) but also for $\Delta\mu$ (0.80 [D / f]). The obtained relatively small magnitude of $\Delta\mu$ (0.80 [D / f]) in fact indicates that, unlike FCPp and FCPa, the F state of unquenched FCPb possesses non negligible CT character. On the other hand, the analysis of QFCPb yields almost the same magnitude of ZDC for both b2b (−0.0297 at 1 MV cm^{-1}) and b3b (−0.0285 at 1 MV cm^{-1}), whereas the values of $\Delta\alpha$ and $\Delta\mu$ for b3b are found to be 5 (=35.79 / 7.16) and 3 (=1.38 / 0.46) times larger compared to the ones obtained for b2b. Besides, the magnitudes of ZDC estimated for b2b (0.0297 at 1 MV cm^{-1}) is more than two times larger in QFCPb than in FCPb (0.0115 at 1 MV cm^{-1}). Therefore, unlike FCPp or FCPa, aggregation of FCPb results in a single species giving the emission band b3b and the addition of the b4p/b4a like band only leads to a slight improvement of the fit. The analysis of the SF spectrum reveals that, similarly to the b3p and b3a bands of QFCPp and QFCPa, the species giving rise to the b3b in QFCPb band has moderately large CT character.

4. Discussion

Our results from SF spectroscopy have revealed two distinct emitting pigment species associated with the quenched state in aggregated FCPp and FCPa, and one species in FCPb. The first species that has its emission peak at 690–692 nm is common to all three (aggregated) FCP samples. We suggest this band to originate from interacting Chl pigments, the emission of which is redshifted with respect to the corresponding unquenched samples, and broadened due to the mixing with a CT-state. It is worth mentioning that transient absorption results on FCP preparations show systematic changes in the Chl a band(s) in the 680 to 740 nm region upon induction of the quenched state by
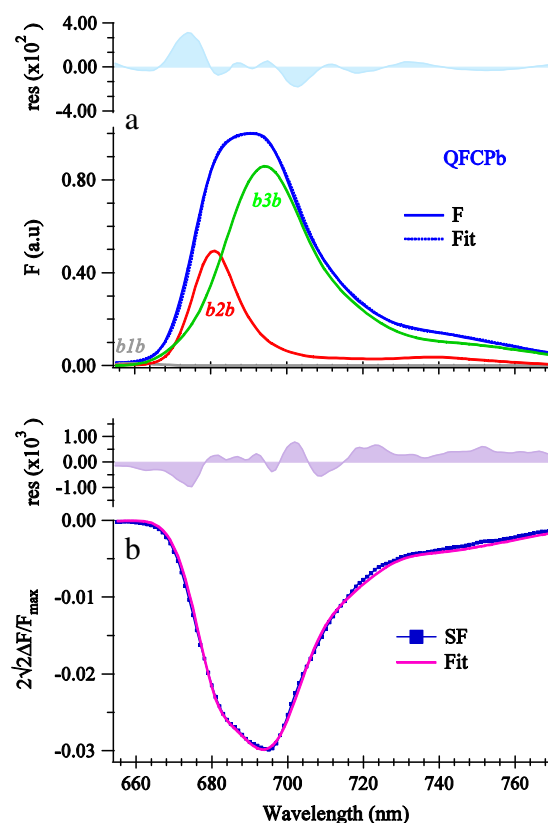
aggregation (Ramanan, Berera, unpublished results). Unlike LHCII, these interacting Chls do not display strongly red shifted fluorescence. The Chls responsible for this emission band may directly act as quenchers in a process similar to that of concentration quenching [32–34], and/or open up an energy transfer channel via a low-lying dark state of a neighboring carotenoid which in turn would dissipate energy [35]. Note that, in our modeling scheme, the emission profile of the first aggregated species (b3 band) has a rather large inhomogeneously broadened lineshape and is composed of five Gaussians. One may infer that the five Gaussians reflect a gradient of aggregation states leading to progressively red-shifted emission. To this end it is worth noting that if the five Gaussians are not linked in the analysis, i.e. they are let free, essentially the same set of molecular parameters (ZDC, $\Delta\alpha$ and $\Delta\mu$) is obtained for each subband. This suggests that the five Gaussians are associated to the same band rather than with a gradient of FCP subpopulation with different degrees of quenching.

The second band emitting in the longer wavelength region is present in both QFCPp and QFCPa, but could not be clearly resolved in QFCPb; this suggests that in QFCPp it is formed upon aggregation of the FCPa

Table 1
Estimated molecular parameters for FCPp.

Sample	Band	λ_{max} [nm]	FWHM [nm]	ZDC [at 1 MV cm^{-1}]	$\Delta\alpha$ [Å^3 / f^2]	$\Delta\mu$ [D/f]
FCPp	Single	675	15	−0.0033	7.16	0.00
QFCPp	b2p	680	15	−0.015	−7.16	0.00
	b3p	692	30	−0.032	−10.74	1.03
	b4p	736	36	−0.0005	−214.75	8.00

ZDC—Zeroth Derivative Contribution.

Table 2
Estimated molecular parameters for FCPa.

Sample	Band	λ_{max} [nm]	FWHM [nm]	ZDC [at 1 MV cm^{-1}]	$\Delta\alpha$ [$\mathring{A}^3 / f^2$]	$\Delta\mu$ [D / f]
FCPa	Single	677	15	−0.011	12.54	0.00
QFCPa	b2a	682	15	−0.071	−10.74	0.00
	b3a	692	31	−0.071	−25.05	2.53
	b4a	740	35	−0.022	−286.33	11.30

ZDC—Zeroth Derivative Contribution.

fraction present in the FCP pool. The analysis of the SF spectrum reveals that the species giving emission in the longer wavelength region has remarkably large CT parameters ($\Delta\alpha$ and $\Delta\mu$). This band, which is characterized by red shifted emission and a broad spectral shape, displays features very similar to those we detected in the dissipative state of the major light harvesting antenna of plants, LHCII, thus pointing to a common quenching mechanism [26]. The new band shows very low fluorescence yield which suggests that non-emissive states may be involved in its formation. In our previous work we proposed it to originate from a Chl–Car mixed excitonic-CT state in the terminal emitter of LHCII. The similarity of the red band we detected in this study with the one we found in LHCII points to the same origin in the two systems. Thus we suggest it to originate from Chl–Car interaction in FCP. FCPa is known to bind diadino- and diatoxanthin in small amounts, depending on the light intensity the cells have experienced during growth [3]. In FCPp more of these carotenoids is retained [12]. However, since the red band is very similar in FCPp and FCPa, and hardly detectable in FCPb, neither diadinoxanthin nor diatoxanthin are likely to be responsible for the red emission. It has recently been shown that two fucoxanthin pools in FCP are active in triplet–triplet energy transfer [36]. It is possible that the vicinity and orientation of one or more Chls to a fucoxanthin pigment is such that a small conformational change may induce a Chl–Car interaction responsible for the red shifted emission band that we detected here and for energy dissipation. Fucoxanthin is characterized by a strong intramolecular charge transfer (ICT) state in its excited state manifold coupled to the S_1 state. This S_1/ICT state has been shown to be active in energy transfer to neighboring Chls in two fucoxanthin pools in FCP [7]. Besides their pivotal role in light harvesting in marine photosynthesis [37–39], carotenoid ICT states have been shown to act as a mediator in the energy dissipation process in biomimetic energy dissipating devices [35] and the same mechanism has been proposed to be active in different photosynthetic organisms [16,40,41]. More recently it was shown that low-lying carotenoid excited states can couple with the Q_y state of a neighboring tetrapyrrole opening up an energy dissipation channel [42] and there is evidence that such mechanism may be active in vivo [43]. We propose that the red shifted (b4) band we detected in the quenched FCP preparations originates from the interaction between the fucoxanthin S_1/ICT state and the Q_y state of one or more neighboring Chl(s). Such state would act as an energy sink and energy dissipator. The lack of evidence for excitonically coupled Chl pairs equivalent to those in LHCII [1,44–46] in FCPs argues against a Chl–Chl CT state being responsible for the red emission of the b4 band.

NPQ in diatoms was shown to depend on the presence of the Lhcx proteins and on the diatoxanhtin content. Indeed, one of the major differences between FCPa and FCPb is the presence of Lhcx polypeptides in

the former. Only for FCPa it was shown earlier that its fluorescence yield depends on the amount of bound diatoxanthin. A model relating these features and the aggregation dependence of the fluorescence yield of FCPa to the in vivo situation in *C. meneghiniana* was proposed by Grouneva et al. [47]. However, aggregation also reduces the fluorescence yield in FCPb and Miloslavina et al. [17] identified aggregation as one part of NPQ in *C. meneghiniana* in vivo, but it remained unclear whether FCPa, FCPb or both contribute to it. FCPa and FCPb display a high degree of sequence homology, but FCPa binds slightly less Chl a compared to FCPb. On the other hand FCPb binds fucoxanthin in a way that a larger bathochromic shift is induced compared to the carotenoids in FCPa [4]. While our data clearly show a new red emitting band in FCPp and FCPa, this band is not clearly resolved in FCPb. Upon a close look at Fig. 6 it is plausible that a similarly red shifted band is also present in FCPb but with very low yield under our experimental conditions, making it very difficult to detect. This raises the question as to whether different dissipative mechanisms are present in FCPa and FCPb. Single molecule spectroscopy has revealed remarkable flexibility in light-harvesting pigment–protein complexes. Lhca4 has been shown to be able to reversibly switch from a red state to an LHCII-like state [48]. For LHCII it was demonstrated, using the same technique, that different quenching states are reversibly accessible to the molecule. Many of them are characterized by no spectral shift while a small fraction shows different degrees of red shift up to 100 nm with respect to the emission of the unquenched complex [49]. This intrinsic feature of LHCII suggests that the plasticity of the molecule allows it to assume different (molecular) quenching configurations which open up different quenching channels. Our results on bulk FCPp, FCPa and FCPb suggest that the oligomeric state of FCPa and FCPb may be characterized by different quenching mechanisms. We suggest that at least two quenched configurations are accessible to FCPa and FCPb giving rise to the b3 and b4 bands upon aggregation. Oligomerization would shift the equilibrium towards both configurations, i.e towards both dissipative states in FCPa but preferentially to one dissipative state, characterized by the b3 band, in FCPb. It has been shown that for the (red) fucoxanthin pool carotenoid to Chl a energy transfer is more efficient in FCPa than in FCPb [7]. It is plausible that for this reason the quenched state associated to the b4 band is more accessible in FCPa than it is in FCPb and thus the new red shifted band could be clearly identified in FCPa but not in FCPb. Such state may however be accessible in vivo for both FCPa and FCPb and possibly in vitro under different experimental conditions and thus constitute an energy dissipation channel in both FCPa and FCPb upon aggregation. Transient absorption and single molecule spectroscopy studies are underway to better understand the biophysical quenching mechanisms in FCP pigment–protein complexes.

Appendix A. Supplementary data

Supplementary data to this article can be found online at http://dx.doi.org/10.1016/j.bbabio.2013.09.001.

Table 3
Estimated molecular parameters for FCPb.

Sample	Band	λ_{max} [nm]	FWHM [nm]	ZDC [at 1 MV cm^{-1}]	$\Delta\alpha$ [$\mathring{A}^3/f^2$]	$\Delta\mu$ [D/f]
FCPb	Single	677	15	−0.0115	10.74	0.80
QFCPb	b2b	681	15	−0.0297	−7.16	0.46
	b3b	694	27	−0.0285	−35.79	1.38

ZDC—Zeroth Derivative Contribution.

References

[1] E. Papagiannakis, et al., Spectroscopic characterization of the excitation energy transfer in the fucoxanthin–chlorophyll protein of diatoms, Photosynth. Res. 86 (1–2) (2005) 241–250.

[2] C. Buchel, Fucoxanthin–chlorophyll proteins in diatoms: 18 and 19 kDa subunits assemble into different oligomeric states, Biochemistry 42 (44) (2003) 13027–13034.

[3] A. Beer, et al., Subunit composition and pigmentation of fucoxanthin–chlorophyll proteins in diatoms: evidence for a subunit involved in diadinoxanthin and diatoxanthin binding, Biochemistry 45 (43) (2006) 13046–13053.

[4] L. Premvardhan, et al., Carotenoid structures and environments in trimeric and oligomeric fucoxanthin chlorophyll a/c(2) proteins from resonance Raman spectroscopy, J. Phys. Chem. B 113 (37) (2009) 12565–12574.

[5] L. Premvardhan, et al., Pigment organization in fucoxanthin chlorophyll a/c(2) proteins (FCP) based on resonance Raman spectroscopy and sequence analysis, Biochim. Biophys. Acta Bioenerg. 1797 (8) (2010) 1647–1656.

[6] L. Premvardhan, et al., The charge–transfer properties of the S-2 state of fucoxanthin in solution and in fucoxanthin chlorophyll-a/c(2) protein (FCP) based on Stark spectroscopy and molecular–orbital theory, J. Phys. Chem. B 112 (37) (2008) 11838–11853.

[7] N. Gildenhoff, et al., Oligomerization and pigmentation dependent excitation energy transfer in fucoxanthin–chlorophyll proteins, Biochim. Biophys. Acta Bioenerg. 1797 (5) (2010) 543–549.

[8] A.V. Ruban, et al., Long-wavelength chlorophyll species are associated with amplification of high-energy-state excitation quenching in higher-plants, Biochim. Biophys. Acta 1059 (3) (1991) 355–360.

[9] A.V. Ruban, et al., The super-excess energy dissipation in diatom algae: comparative analysis with higher plants, Photosynth. Res. 82 (2) (2004) 165–175.

[10] J. Lavaud, et al., Influence of the diadinoxanthin pool size on photoprotection in the marine planktonic diatom *Phaeodactylum tricornutum*, Plant Physiol. 129 (3) (2002) 1398–1406.

[11] B. Bailleul, et al., An atypical member of the light-harvesting complex stress-related protein family modulates diatom responses to light, Proc. Natl. Acad. Sci. U. S. A. 107 (42) (2010) 18214–18219.

[12] K. Gundermann, C. Buechel, The fluorescence yield of the trimeric fucoxanthin–chlorophyll-protein FCPa in the diatom *Cyclotella meneghiniana* is dependent on the amount of bound diatoxanthin, Photosynth. Res. 95 (2–3) (2008) 229–235.

[13] K. Gundermann, C. Buechel, Factors determining the fluorescence yield of fucoxanthin–chlorophyll complexes (FCP) involved in non-photochemical quenching in diatoms, Biochim. Biophys. Acta Bioenerg. 1817 (7) (2012) 1044–1052.

[14] P. Horton, A.V. Ruban, R.G. Walters, Regulation of light harvesting in green plants, Annu. Rev. Plant Physiol. Plant Mol. Biol. 47 (1996) 655–684.

[15] P. Horton, et al., Control of the light-harvesting function of chloroplast membranes by aggregation of the LHCII chlorophyll protein complex, FEBS Lett. 292 (1–2) (1991) 1–4.

[16] A.V. Ruban, et al., Identification of a mechanism of photoprotective energy dissipation in higher plants, Nature 450 (7169) (2007) 575–579.

[17] Y. Miloslavina, et al., Ultrafast fluorescence study on the location and mechanism of non-photochemical quenching in diatoms, Biochim. Biophys. Acta Bioenerg. 1787 (10) (2009) 1189–1197.

[18] G.U. Bublitz, S.G. Boxer, Stark spectroscopy: applications in chemistry, biology, and materials science, Annu. Rev. Phys. Chem. 48 (1997) 213–242.

[19] M. Wahadoszamen, et al., External electric field effects on absorption, fluorescence, and phosphorescence spectra of diphenylpolyynes in a polymer film, J. Phys. Chem. A 111 (38) (2007) 9544–9552.

[20] M. Wahadoszamen, et al., External electric field effects on absorption and fluorescence spectra of a fullerene derivative and its mixture with zinc-tetraphenylporphyrin doped in a PMMA film, J. Phys. Chem. B 110 (41) (2006) 20354–20361.

[21] M. Wahadoszamen, T. Nakabayashi, N. Ohta, External electric field effects on emission of a mixture of tetraphenylporphyrin and fullerene doped in a polymer film, J. Chin. Chem. Soc. 53 (1) (2006) 85–92.

[22] L. Premvardhan, et al., The charge-transfer character of the $S_0 \rightarrow S_2$ transition in the carotenoid peridinin is revealed by Stark spectroscopy, J. Phys. Chem. B 109 (32) (2005) 15589–15597.

[23] A.M. Ara, et al., External electric field effects on fluorescence of pyrene butyric acid in a polymer film: concentration dependence and temperature dependence, J. Phys. Chem. B 110 (47) (2006) 23669–23677.

[24] T. Nakabayashi, M. Wahadoszamen, N. Ohta, External electric field effects on state energy and photoexcitation dynamics of diphenylpolyenes, J. Am. Chem. Soc. 127 (19) (2005) 7041–7052.

[25] T. Iimori, et al., Remarkable temperature dependence of electric field-induced change in fluorescence spectra of pyrene doped in a polymer matrix, Chem. Phys. Lett. 402 (1–3) (2005) 206–211.

[26] M. Wahadoszamen, et al., Identification of two emitting sites in the dissipative state of the major light harvesting antenna, Phys. Chem. Chem. Phys. 14 (2) (2012) 759–766.

[27] L. Provasoli, J.J.A. McLaughlin, M.R. Droop, The development of artificial media for marine algae, Arch. Mikrobiol. 25 (4) (1957) 392–428.

[28] F. van Mourik, et al., Direct observation of solvation dynamics and dielectric relaxation in the photosynthetic light-harvesting-2 complex of *Rhodopseudomonas acidophila*, J. Phys. Chem. B 107 (9) (2003) 2156–2161.

[29] D.S. Gottfried, J.W. Stocker, S.G. Boxer, Stark-effect spectroscopy of bacteriochlorophyll in light-harvesting complexes from photosynthetic bacteria, Biochim. Biophys. Acta 1059 (1) (1991) 63–75.

[30] A. Moscatelli, et al., Electric-field-induced fluorescence quenching in polyfluorene, ladder-type polymers, and MEH-PPV: evidence for field effects on internal conversion rates in the low concentration limit, J. Phys. Chem. B 114 (45) (2010) 14430–14439.

[31] K.A. Walters, D.A. Gaal, J.T. Hupp, Interfacial charge transfer and colloidal semiconductor dye-sensitization: mechanism assessment via Stark emission spectroscopy, J. Phys. Chem. B 106 (20) (2002) 5139–5142.

[32] M.G. Mueller, et al., Singlet energy dissipation in the photosystem II light-harvesting complex does not involve energy transfer to carotenoids, Chemphyschem 11 (6) (2010) 1289–1296.

[33] W.F. Watson, R. Livingston, Concentration quenching of fluorescence in chlorophyll solutions, Nature 162 (4116) (1948) 452–453.

[34] G.S. Beddard, G. Porter, Concentration quenching in chlorophyll, Nature 260 (5549) (1976) 366–367.

[35] R. Berera, et al., A simple artificial light-harvesting dyad as a model for excess energy dissipation in oxygenic photosynthesis, Proc. Natl. Acad. Sci. U. S. A. 103 (14) (2006) 5343–5348.

[36] M. Di Valentin, et al., Chlorophyll triplet quenching by fucoxanthin in the fucoxanthin–chlorophyll protein from the diatom *Cyclotella meneghiniana*, Biochem. Biophys. Res. Commun. 427 (3) (2012) 637–641.

[37] J.A. Bautista, et al., Excited state properties of peridinin: observation of a solvent dependence of the lowest excited singlet state lifetime and spectral behavior unique among carotenoids, J. Phys. Chem. B 103 (41) (1999) 8751–8758.

[38] D. Zigmantas, et al., Carotenoid to chlorophyll energy transfer in the peridinin–chlorophyll-a-protein complex involves an intramolecular charge transfer state, Proc. Natl. Acad. Sci. U. S. A. 99 (26) (2002) 16760–16765.

[39] I.H.M. van Stokkum, et al., Inter-pigment interactions in the peridinin chlorophyll protein studied by global and target analysis of time resolved absorption spectra, Chem. Phys. 357 (1–3) (2009) 70–78.

[40] R. Berera, et al., A mechanism of energy dissipation in cyanobacteria, Biophys. J. 96 (6) (2009) 2261–2267.

[41] R. Berera, et al., The photophysics of the orange carotenoid protein, a light-powered molecular switch, J. Phys. Chem. B 116 (8) (2012) 2568–2574.

[42] M. Kloz, et al., Carotenoid photoprotection in artificial photosynthetic antennas, J. Am. Chem. Soc. 133 (18) (2011) 7007–7015.

[43] S. Bode, et al., On the regulation of photosynthesis by excitonic interactions between carotenoids and chlorophylls, Proc. Natl. Acad. Sci. U. S. A. 106 (30) (2009) 12311–12316.

[44] V.I. Novoderezhkin, et al., Excitation dynamics in the LHCII complex of higher plants: modeling based on the 2.72 Angstrom crystal structure, J. Phys. Chem. B 109 (20) (2005) 10493–10504.

[45] F. Muh, M.E.-A. Madjet, T. Renger, Structure-based identification of energy sinks in plant light-harvesting complex II, J. Phys. Chem. B 114 (42) (2010) 13517–13535.

[46] G. Zucchelli, S. Santabarbara, R.C. Jennings, The Qy absorption spectrum of the light-harvesting complex II as determined by structure-based analysis of chlorophyll macrocycle deformations, Biochemistry 51 (13) (2012) 2717–2736.

[47] I. Grouneva, et al., Influence of ascorbate and pH on the activity of the diatom xanthophyll cycle-enzyme diadinoxanthin de-epoxidase, Physiol. Plant. 126 (2) (2006) 205–211.

[48] T.P.J. Kruger, et al., Conformational switching explains the intrinsic multifunctionality of plant light-harvesting complexes, Proc. Natl. Acad. Sci. U. S. A. 108 (33) (2011) 13516–13521.

[49] T.P.J. Kruger, et al., Controlled disorder in plant light-harvesting complex II explains its photoprotective role, Biophys. J. 102 (11) (2012) 2669–2676.